Environmental Modelling & Software 80 (2016) 322–335

Contents lists available at ScienceDirect

Environmental Modelling & Software

journal homepage: www.elsevier.com/locate/envsoft

Performance assessment of OpenFOAM and FLOW-3D in the numerical modeling of a low Reynolds number hydraulic jump

Arnau Bayon [a], Daniel Valero [b], Rafael García-Bartual [a], Francisco José Vallés-Morán [a], P. Amparo López-Jiménez [a, *]

[a] Universitat Politècnica de València, Camí de Vera, s/n, València, 46022, Spain
[b] FH Aachen University of Applied Sciences, Bayernallee, 9, Aachen, 52066, Germany

ARTICLE INFO

Article history:
Received 26 June 2015
Received in revised form
5 February 2016
Accepted 10 February 2016
Available online 23 March 2016

Keywords:
CFD
RANS
OpenFOAM
FLOW-3D
Hydraulic jump
Air–water flow
Low Reynolds number

ABSTRACT

A comparative performance analysis of the CFD platforms OpenFOAM and FLOW-3D is presented, focusing on a 3D swirling turbulent flow: a steady hydraulic jump at low Reynolds number. Turbulence is treated using RANS approach RNG k-ε. A Volume Of Fluid (VOF) method is used to track the air–water interface, consequently aeration is modeled using an Eulerian–Eulerian approach. Structured meshes of cubic elements are used to discretize the channel geometry. The numerical model accuracy is assessed comparing representative hydraulic jump variables (sequent depth ratio, roller length, mean velocity profiles, velocity decay or free surface profile) to experimental data. The model results are also compared to previous studies to broaden the result validation. Both codes reproduced the phenomenon under study concurring with experimental data, although special care must be taken when swirling flows occur. Both models can be used to reproduce the hydraulic performance of energy dissipation structures at low Reynolds numbers.

1. Introduction

A hydraulic jump is the abrupt transition from supercritical to subcritical flow (Fig. 1). It constitutes a highly chaotic phenomenon characterized by large turbulent fluctuations of velocity and pressure, air entrainment and energy dissipation. Hydraulic jumps are usually described in terms of the well-known Froude number (Fr_i) which, in rectangular channels at a given section "i", is computed as follows:

$$Fr_i = \frac{u_i}{\sqrt{g\ y_i}} \quad (1)$$

Where y_i, is water depth, u_i is depth-averaged velocity, and g is gravity acceleration. One of the most interesting aspects of hydraulic jumps is that, despite their chaotic nature, some of their properties remain steady within a certain range of approaching Froude numbers (Fr_1). This allows studying some representative features, such as the jump toe position (flow impingement location) or the roller length (stretch downstream of the jump toe where flow recirculates). Some of these phenomena behave in a quasi-periodic fashion and so can be analyzed statistically (Wang and Chanson, 2015a; Wang et al., 2014a; Mossa, 1999).

Since first known hydraulic jump experiences (Bidone, 1819; Belanger, 1841), a wealth of studies on this topic has been conducted. One of the main reasons is that hydraulic jumps are the most used method to dissipate energy in hydraulic structures (Chow, 1959). Classic literature on the area states that approaching Froude numbers between 4.5 and 9.0 yield stabilized hydraulic jumps, least dependent on tailwater variations (Peterka, 1984; Hager, 1992). Lower values of Fr_1 lead to undular or transition jumps, characterized by lower efficiencies and formation of waves of irregular period (Fawer, 1937; Chow, 1959; Chanson and Montes, 1995). Higher values of Fr_1 produce choppy jumps, where flow detachment, as well as bubble and spray formation are frequent. For these reasons, the U.S. Bureau of Reclamation (Peterka, 1984) recommends designing energy dissipation structures so that only steady hydraulic jumps occur.

The first known study reporting turbulence quantities in

* Corresponding author. Hydraulic and Environmental Engineering Department, Universitat Politècnica de València, Camino de Vera s/n, 46022, Valencia, Spain. Tel.: +34 630831608; fax: +34 963877981.
E-mail addresses: arbabar@iiama.upv.es (A. Bayon), palopez@upv.es (P.A. López-Jiménez).

http://dx.doi.org/10.1016/j.envsoft.2016.02.018
1364-8152/

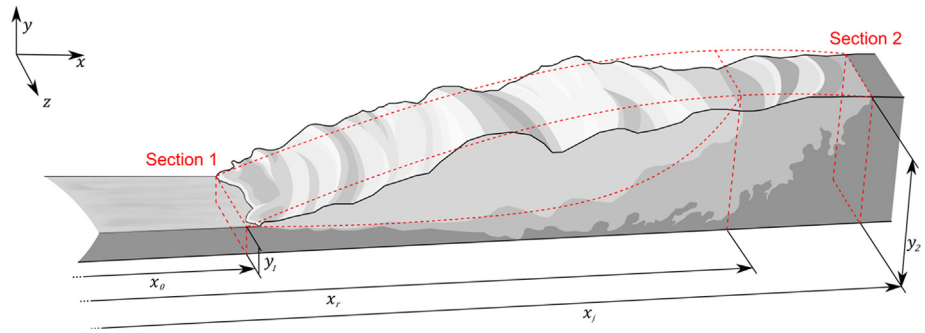

Fig. 1. Hydraulic jump flow structure.

hydraulic jumps was conducted by Rouse et al. (1959) and was later completed by Rajaratnam (1965) and Long et al. (1991). On the flow structure description, Resch and Leutheusser (1972) also reported turbulence quantities and pointed out dependence on the inlet flow conditions. Gualtieri and Chanson (2007, 2010) further analyzed the inlet sensitivity conditions and Liu et al. (2004) provided a complete turbulence description for low Froude numbers. Additionally, Chanson & Brattberg (2000), Murzyn et al. (2005), Chanson and Gualtieri (2008), and Zhang et al. (2014) focused on the flow aeration properties. Recently, Wang & Chanson (2015b), Wang et al. (2014b), Zhang et al. (2013), Chachereau and Chanson (2011), Murzyn et al. (2007), and Chanson (2007) reported turbulent integral length and time scales, which might contribute to a better validation and understanding of numerical models.

Given the nature of experimental techniques (Bung, 2013; Borges et al., 2010; Matos et al., 2002), Computational Fluid Dynamics (CFD) can supplement and assist in the design of energy dissipation structures (Bombardelli, 2012; Meireles et al., 2014; Chanson and Carvalho, 2015). Nevertheless, mathematical models still present accuracy issues when modeling some hydraulic phenomena (Blocken and Gualtieri, 2012; Murzyn and Chanson, 2009a), to which the lack of validation is usually pointed out (Chanson, 2013; Chanson and Lubin, 2010). Carvalho et al. (2008) and Ma et al. (2011), among others, managed to reproduce the hydraulic jump structure using different CFD approaches. Caisley et al. (1999) accurately modeled a hydraulic jump using FLOW-3D. Bayon and Lopez-Jimenez (2015), Romagnoli el al. (2009), and Witt et al. (2015) used OpenFOAM to successfully model hydraulic jumps as well.

Numerical approaches different from CFD have also been used to model hydraulic jumps, such as Smoothed Particle Hydrodynamics (De Padova et al., 2013) or Artificial Neural Networks (Omid et al., 2005). Other authors preferred one-dimensional and two-dimensional models to study the hydraulic behavior of rivers or stilling basins and erosion-sedimentation phenomena (Hartanto et al., 2011; Dewals et al., 2004; Juez et al., 2013). Nevertheless, flows occurring in hydraulic structures tend to be highly three-dimensional (Ahmed and Rajaratnam, 1997; Chanson and Montes, 1995). For this reason, the use of three-dimensional models, such as that proposed in this paper, becomes a must in most cases.

In real life applications, choosing the most suitable numerical model when facing fluid mechanics problems can be a tedious and confusing task given the large amount of possible choices. As stated above, two of the most widely used CFD codes in hydraulic engineering applications are the open source platform OpenFOAM and the commercial software FLOW-3D. The main goal of this paper is to conduct a systematic comparison between them in terms of accuracy. To do so, a RANS model for classical hydraulic jumps is set similarly in OpenFOAM and FLOW-3D using the RNG k–ε turbulence model (Yakhot et al., 1992) and a two-phase VOF approach (Hirt and Nichols, 1981). A case study based on a steady hydraulic jump (Fr_1~6) of low Reynolds number (Re_1=30,000) is simulated. For validation purposes, the results are compared to data obtained using an open channel physical model and previous authors' experimental studies. Additionally, sensitivity to certain parameters, such as mesh refinement and time-averaging window size, is also assessed. Low Reynolds number might prevent from extrapolating present results to prototype scale structures where air–water flows prevail and Reynolds numbers are 2–4 orders of magnitude larger.

2. Numerical model

The present model is implemented using two widespread numerical codes, namely: OpenFOAM and FLOW-3D. OpenFOAM (2011) is a freely available open source platform containing several C++ libraries and applications which can numerically solve continuum mechanics problems (Weller et al., 1998). Its implementation is based on a tensorial approach using object-oriented programming techniques and the Finite Volume Method or FVM (McDonald, 1971). FLOW-3D is a commercial software package based as well on the FVM, developed by FlowScience, Inc. FLOW-3D includes the Volume of Fluid (VOF) method as originally described by Hirt and Nichols (1981). FLOW-3D allows using one-fluid approach for free surface flows (Prosperetti and Tryggvason, 2007; Bombardelli et al., 2011; Oertel and Bung, 2012) although this approach is not used in this study. This code has been widely used in hydraulic applications since it was released in 1986. In this section, an in-depth discussion on the proposed model implementation using both CFD platforms used is presented. Special attention is paid to those aspects where the OpenFOAM and FLOW-3D approaches differ (see Table 1).

2.1. Geometry and mesh

According to the definition of classical hydraulic jump, the discretized spatial domain is rather simple: it consists of a horizontal rectangular channel. Unstructured meshes would allow a selective refinement of regions where large gradients of flow variables are expected (Kim and Boysan, 1999). Furthermore, their arbitrary topology makes them fit better into complex geometries as well as show fewer closure issues (Biswas and Strawn, 1998). However, none of these facts implies an advantage in the case of this study, as the modeled geometry constitutes one of the simplest possible cases.

However, according to Biswas and Strawn (1998) and Hirsch (2007), structured meshes are generally more accurate than unstructured meshes. In addition, their algorithms tend to be more

Table 1
Summary of numerical model setup according to the code used.

	OpenFOAM	FLOW-3D
Mesh	3D structured (cubic cells)	3D structured (cubic cells)
Turbulence model	RANS RNG k–ε	RANS RNG k–ε
Solid contours	No slip, smooth surface, high *Re* wall function	No slip, smooth surface, high *Re* wall function
Advection scheme	Explicit 2nd order limited (Van Leer, 1977)[a]	Explicit 2nd order limited (Van Leer, 1977)
Diffusion scheme	Explicit 2nd order	Explicit 2nd order
Courant number limit	0.75	0.75
Multiphase treatment	VOF with two fluids	VOF with two fluids
Free surface tracking	Interface compression velocity (Ubbink, 1997)	Donor-acceptor method (Hirt and Nichols, 1981)
Aeration	Eulerian–Eulerian approach	Eulerian–Eulerian approach

[a] In OpenFOAM, scalar variables with no abrupt gradients, such as k or ε, are discretized using an explicit 1st order scheme.

straight forward and faster. Also structured meshes produce a more regular access to memory and so lower the latency of simulations (Keyes et al., 2000). Besides, topologically orthogonal meshes tend to cause less numerical issues in multiphase flows. As a consequence, a structured rectangular hexahedral mesh is considered more suitable to the problem in this study.

Thus, uniform cubic mesh elements of size Δx are used to discretize the channel (see Fig. 2) which may yield higher order of accuracy as higher order errors are neglected in some numerical schemes (Hirsch, 2007). The optimum mesh element size is case specific. Hence, it must be determined by means of a mesh sensitivity analysis, described below.

2.2. Flow equations

A complete description of flows with breaking free surfaces, air entrapment and three-dimensional flow patterns cannot be achieved using shallow water approaches, such as Saint-Venant (1871) or Boussinesq (1871). In these cases, a full description of the flow characteristics requires the use of the Navier–Stokes Equations (Eqs. (2) and (3)). In their general form, these equations govern fluid motion. Despite the VOF method can be applied to variable-density flows (Chen and Li, 1998), in this particular case Navier–Stokes equations are used in their incompressible form (this assumption can generally be done in flows where the Mach number is Ma<0.3). For the numerical solution of the flow equations, the Finite Volume Method (FVM) has been employed.

$$\nabla \bar{u} = 0 \tag{2}$$

$$\frac{\partial \bar{u}}{\partial t} + \bar{u}\cdot\nabla\bar{u} = -\frac{1}{\rho}\nabla p + \upsilon\nabla^2\bar{u} + \overline{f_b} \tag{3}$$

Where u is velocity, p is pressure, ρ is density, υ is kinematic viscosity, $\overline{f_b}$ is body forces (gravity and surface tension); and t is time. Concerning time discretization, the time step length is automatically adjusted in order to ensure that Courant numbers remain below a threshold of Cr<0.75.

2.3. Free surface modeling

The way that the coexistence of several fluids is treated is of paramount importance in multiphase flow numerical modeling. The stability and accuracy of the algorithm used to define the interface between fluid phases proved to exert a significant effect on the final model outcome (Hyman, 1984). A large number of surface tracking approaches has been reported since the first Lagrangian model proposed by Daly (1969). Among all these, Eulerian–Eulerian methods are generally preferred in models like that presented herein, as discussed in Bayon and Lopez-Jimenez (2015). These kind of methods are comparatively computationally more efficient since, unlike Lagrangian approaches, they only use a single variable value in every mesh element (Ubbink, 1997). This scalar variable (α) expresses the fraction of one fluid contained at each mesh element. When only two fluids are modeled, both fluid fractions are complementary. An additional transport equation must be approximated to determine the value of the fluid fraction throughout the computational domain (Hirt and Nichols, 1981):

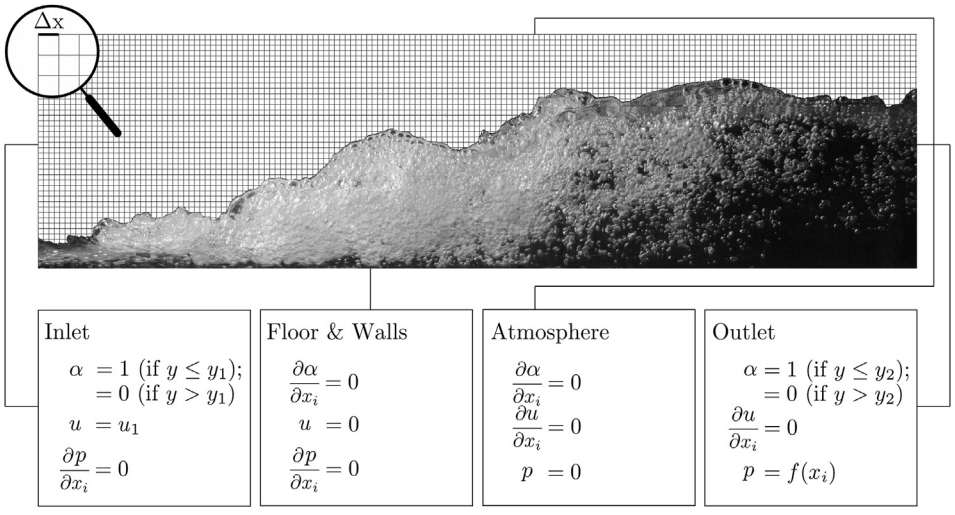

Fig. 2. Mesh overlapping a hydraulic jump snapshot and description of the boundary conditions.

$$\frac{\partial \alpha}{\partial t} + \nabla \cdot (\overline{u}\alpha) = 0 \quad (4)$$

Where α is fluid fraction, u is velocity, and t is time. It is important to remark that this approach considers both fluids, say A and B, to be a single multiphase fluid. The transport of other properties (ξ) is treated by means of weighted averages, according to the fluid fraction in each mesh element:

$$\xi = \xi_A \alpha + \xi_B (1 - \alpha) \quad (5)$$

As a result, a set of values between 0 and 1 is obtained but no neat fluid interface is explicitly defined. Different methods for this purpose have been reported during the last decades. Line techniques, e.g. SLIC (Noh and Woodward, 1976), PLIC (Youngs, 1984) or FLAIR (Ashgriz and Poo, 1991), were the first viable approaches in this regard. Nevertheless, problems of generalization to unstructured meshes made them fall into disuse. The so-called donor-acceptor methods, such as the VOF (Hirt and Nichols, 1981), implemented in FLOW-3D, have been widely used, although they used to depict false interface deformation issues. Higher order differencing schemes were aimed to overcome these problems, although they still can suffer from surface smearing and numerical diffusion issues, leading to spurious currents in the vicinity of fluid interfaces (Ubbink, 1997). As regards OpenFOAM, an interface compression algorithm is implemented to avoid the aforementioned problems. This is achieved by adding an extra term to the left hand side of Eq. (4): $\nabla \cdot (\overline{u_c}\ \alpha\ [1-\alpha])$, where $\overline{u_c}$ is an arbitrarily defined compression velocity term to which the direction is perpendicular to the fluid interface. This term is multiplied by $\alpha\ [1-\alpha]$ to ensure that it will only be relevant in zones where the fluid fraction variable is close to 0.5 (where the fluid interfaces are defined). A more in-depth discussion on this topic can be found in Rusche (2002) and Berberovic (2010).

2.4. Flow aeration

In air–water flows, aeration induces volume bulking, increases flow depth, adds compressibility to the flow and modifies its macroscopic density (Chanson, 2013; Falvey, 1980), thus affecting momentum distribution of the carrier phase. Flow aeration also bounds scour phenomena caused by cavitation (Bung and Schlenkhoff, 2010; Wood, 1991; Pfister, 2011) and shear stresses on the channel boundaries (Chanson, 1994). A stable and accurate method to treat this phenomenon is of paramount importance when dealing with bores, breaking waves or hydraulic jumps. Unfortunately, no method *per se* can accurately reproduce phenomena with a characteristic length scale smaller than mesh elements, e.g. bubbles or droplets (Valero and Bung, 2015; Lobosco et al., 2011; Toge, 2012).

Subscale air-entrainment models can be implemented in order to overcome this issue (Valero and Garcia-Bartual, 2016; Ma et al., 2011). In low-aerated flows, Eulerian-Lagrangian approaches are a good choice. These methods consist of the approximation of the Navier–Stokes Equations, while air bubbles are treated as flow-driven discrete particles. However, this approach becomes computationally expensive in highly aerated flows. In these cases, Eulerian–Eulerian methods arise as an efficient approach. An entirely Eulerian method with two fluids has been used in the present study, allowing both fluids to mix in the same cell but locating the free surface where $\alpha = 0.5$. However no additional equation is employed for bubble and droplet dynamics. A detailed discussion on more advanced methods can be found in Balachandar and Eaton (2010).

2.5. Turbulence modeling

One of the key aspects of CFD models is the way turbulence is treated. Velocity and pressure fluctuations can be numerically resolved down to their lowest scales (Direct Numerical Simulation or DNS) as long as the mesh is accordingly fine (Pope, 2000; Hirsch, 2007). However, this approach is still unaffordable in terms of computational cost for any engineering application. The use of DNS in multiphase flows has been reported in the literature (Prosperetti and Tryggvason, 2007; Borue et al., 1995; Nagaosa, 1999), although in engineering applications turbulence is partially modeled.

Large Eddy Simulation (LES) methods offer accurate multiphase flow simulations at lower computational costs, being however still unaffordable for most engineering applications (Spalart, 2000). Thus, the most widely used approach in engineering applications is the Reynolds Averaged Navier–Stokes (RANS). The models of this kind are based on averaging the flow equations yielding the Reynolds Averaged Navier–Stokes (RANS) equations. Further hypothesis are needed for closure. This is commonly achieved by adding transport equations to reproduce the behavior of flow turbulence and then relate the turbulence scales to a turbulent viscosity (μ_t), which is introduced in the flow equations aiming to account for the Reynolds stresses. The first complete models are the two equation models; they are able to provide a full description in turbulence in terms of length and time scales, thus they could reproduce a wide variety of flows (Pope, 2000). An extended description of RANS equations and turbulence closures can be found in Pope (2000) and Wilcox (1998).

The turbulence model used in this study is the RNG k–ε (Yakhot et al., 1992), which usually provides better performance for swirling flows than the standard k–ε model (Bradshaw, 1996; Pope, 2000; Speziale and Thangam, 1992; Kim and Baik, 2004; Bombardelli et al., 2011). Its formulation is depicted in Eqs. (6) and (7):

$$\frac{\partial}{\partial t}(\rho k) + \frac{\partial}{\partial x_i}(\rho k u_i) = \frac{\partial}{\partial x_j}\left[\left(\mu + \frac{\mu_t}{\sigma_k}\right)\frac{\partial k}{\partial x_j}\right] + P_k - \rho\varepsilon \quad (6)$$

$$\frac{\partial}{\partial t}(\rho \varepsilon) + \frac{\partial}{\partial x_i}(\rho \varepsilon u_i) = \frac{\partial}{\partial x_j}\left[\left(\mu + \frac{\mu_t}{\sigma_\varepsilon}\right)\frac{\partial \varepsilon}{\partial x_j}\right] + C_{1\varepsilon}\frac{\varepsilon}{k}P_k - C_{2\varepsilon}\rho\frac{\varepsilon^2}{k} \quad (7)$$

Where k is turbulence kinetic energy (henceforth, TKE), ε is dissipation rate, ρ is density, t is time, x_i is coordinate in the i axis, μ is dynamic viscosity, μ_t is turbulent dynamic viscosity, and P_k is production of TKE. The remaining terms ($C_{1\varepsilon}$, $C_{2\varepsilon}$, σ_k, and σ_ε), are model parameters whose values can be found in Yakhot et al. (1992). Finally, the turbulence viscosity can be computed using the parameter C_μ=0.085:

$$\mu_t = \rho C_\mu \frac{k^2}{\varepsilon} \quad (8)$$

2.6. Boundary conditions

In order to force the hydraulic jump to occur within the modeled channel stretch, a supercritical flow inlet and a subcritical flow outlet are imposed. The desired approaching Froude number is ensured by imposing a constant flow depth at the inlet (y_1) with corresponding velocity value using a Dirichlet boundary condition. Pressure is defined by a null von Neumann boundary condition allowing a hydrostatic profile to develop, which is easily specified in FLOW-3D. In OpenFOAM, this is achieved thanks to the

swak4Foam library. The inlet variables of the RANS model, i.e. k and ε, cannot be defined *a priori* as this is a theoretical case study. Their values at the channel inlet and outlet are set to arbitrary low values so that they can develop while approaching the hydraulic jump. An outlet subcritical flow depth (y_2) has to be imposed so that the hydraulic jump occurs within the simulation domain. This variable cannot be accurately set *a priori* due to the numerous sources of uncertainty and the high sensitivity shown by the jump location. Hence, the subcritical flow depth has to be obtained by iteratively testing values by means of a Dirichlet boundary condition until a compact steady hydraulic jump is formed far enough from both upstream and downstream boundary conditions.

Wall roughness has been neglected given the small roughness of the material of the experimental facility which was used for validation. An atmospheric boundary condition is set to the upper boundary of the channel. This allows the flow to enter and leave the domain as null von Neumann conditions are imposed to all variables except for pressure, which is set to zero (i.e. atmospheric pressure). In Fig. 2 are the summarized boundary conditions which were used.

Boundary layers, the viscous flow region attached to solid boundaries, require special treatment. The so-called universal law of the wall (Von Karman, 1930) describes the flow profiles in such regions. This is achieved through defining a dimensionless velocity (u) and the distance to wall (d) as a function of shear velocity (u_τ) and viscosity (υ):

$$y^+ = d\frac{u_\tau}{\upsilon} \tag{9}$$

Schlichting and Gersten (2000) subdivide boundary layers into three zones according to the shape of their velocity profile: the viscous sub-layer ($y^+<5$) is characterized by a linear correlation between $u^+=u/u_\tau$ and y^+; the buffer sub-layer ($5<y^+<70$), where no analytical profiles are observable as turbulent and laminar features coexist (Olivari and Benocci, 2010); and the logarithmic sub-layer ($y^+>70$), characterized by a full development of turbulence and where TKE production and dissipation terms tend to balance.

It is known that large gradients of property occur in the lowest y^+ regions. For this reason, wall functions can be implemented in CFD codes in order to model these regions instead of directly solving them. This allows the use of coarser meshes, thus saving significant amounts of computational resources. These functions assume that the behavior of viscous sub-layers is universal. Therefore, their main requirement is that mesh elements in contact with solid boundaries must have y^+ values between the buffer and the logarithmic sub-layers (y^+~35).

3. Experimental setup

In order to validate the numerical model outcome, altogether with previous studies, a small scale open channel installed at the Hydraulics Laboratory of the Universitat Politècnica de València (UPV) is used. The device consists of methacrylate walls and a PVC streambed, a recirculation tank and a water pump is employed to provide the desired flow rate. The water pump can reach flow rates up to $4\cdot10^{-3}m^3/s$ (2% uncertainty) and can be maneuvered with a frequency regulator. Given the channel dimensions (3.00m long, 0.10m wide and 0.15m high), Froude numbers spanning from 4.5 to 13 can be obtained. The inlet boundary condition is imposed by an adjustable vertical sluice gate and a jetbox. Both ensure a smooth transition from pressurized to supercritical flow at a desired flow depth. The outlet boundary condition is imposed by a drop-down door, to which the slope can be adjusted to obtain the desired flow depth downstream. Once boundary conditions are set, flow rate and fluid temperature are monitored. Thus, it is ensured that neither flow nor fluid conditions change throughout the test.

In this experimental facility, flow depth measurements are conducted by means of digital image processing. To do so, 10s videos of the hydraulic jump profile are recorded at 50Hz and 1280×720 px ($4.1\cdot10^{-4}$m/px in average, before perspective effect correction). After decomposing videos in frames, flow depth is automatically determined using edge detection tools to track the sudden changes of light intensity that an air–water interfaces cause. Filtering algorithms are applied to raw results to remove the bias caused by reflections, droplets, etc. The water surface tracking provides information on the hydraulic jump profile (Γ) and the supercritical and subcritical flow depths (y_1 and y_2) for comparison with the CFD model outcome. In order to validate the data obtained by digital image treatment, point gauge measurements are simultaneously conducted upstream and downstream of the hydraulic jump.

4. Case study

As stated above, a case study is conducted to assess OpenFOAM and FLOW-3D model accuracy using experimental data and results from previous studies. The case consists of a classical hydraulic jump in a channel of dimensions 1.00m×0.10m×0.15m (length, width and height). Inlet flow is set to $Q=0.003m^3/s$ and supercritical flow depth is set to $y_1=0.013$m, so inlet mean velocity is $u_1=2.308$m/s. The resulting approaching Froude number remains Fr_1~6. Reynolds numbers are Re_1~30,000 and Weber numbers are We~40. According to Hager (1992), these conditions lead to a steady jump. A case study of approaching Froude number (Fr_1) between 6 and 7 is suitable for model validation as it is exactly in the middle of the Fr_1 value span recommended by the U.S. Bureau of Reclamation for stilling basin design (Peterka, 1984). Therefore, this Fr_1 value is considered representative of the behavior of all steady hydraulic jumps within this range. Density and kinematic viscosity are $\rho_w=1000kg/m^3$ and $\upsilon_w=10^{-6}m/s^2$, respectively, for water. For air, $\rho_a=1.20kg/m^3$ and $\upsilon_a=10^{-3}m/s^2$ have been assumed. Despite the air and water temperatures were monitored during the experiments, differences in their properties can occur and so be an additional source of result bias.

Table 2. Description of simulated cases. Specific flow rate (q), inlet mean velocity (v_1), Reynolds number (Re_1) and inlet Froude number (Fr_1).

4.1. Mesh sensitivity analysis

As discussed above, a mesh sensitivity analysis is conducted. To do so, each of the codes (OpenFOAM and FLOW-3D) are tested in five meshes with different cell sizes using sequent depths and roller length as indicators and following the ASME's criteria (Celik et al., 2008). The mesh cell sizes employed are 7.50mm, 5.00mm, 4.00mm, 3.00mm and 1.5mm, being the global refinement ratio 5, way above the recommended minimum value of 1.3 (Celik et al., 2008).

As Fig. 3a and b shows, sequent depths seem to be less sensitive to mesh size than roller lengths. Except for the sequent depth in FLOW-3D, the data analysis demonstrates that oscillatory convergence is reached in mesh sizes below 3mm according to Celik et al. (2008). Fig. 3c corroborates that mesh size has converged and is in the asymptotic range, as the model apparent order approaches the

Table 2
Description of simulated cases. Specific flow rate (q), inlet mean velocity (v_1), Reynolds number (Re_1) and inlet Froude number (Fr_1).

	q [m^2/s]	v_1 [m/s]	Re_1 [-]	Fr_1 [-]
Present study	0.030	2.308	30000	6.5

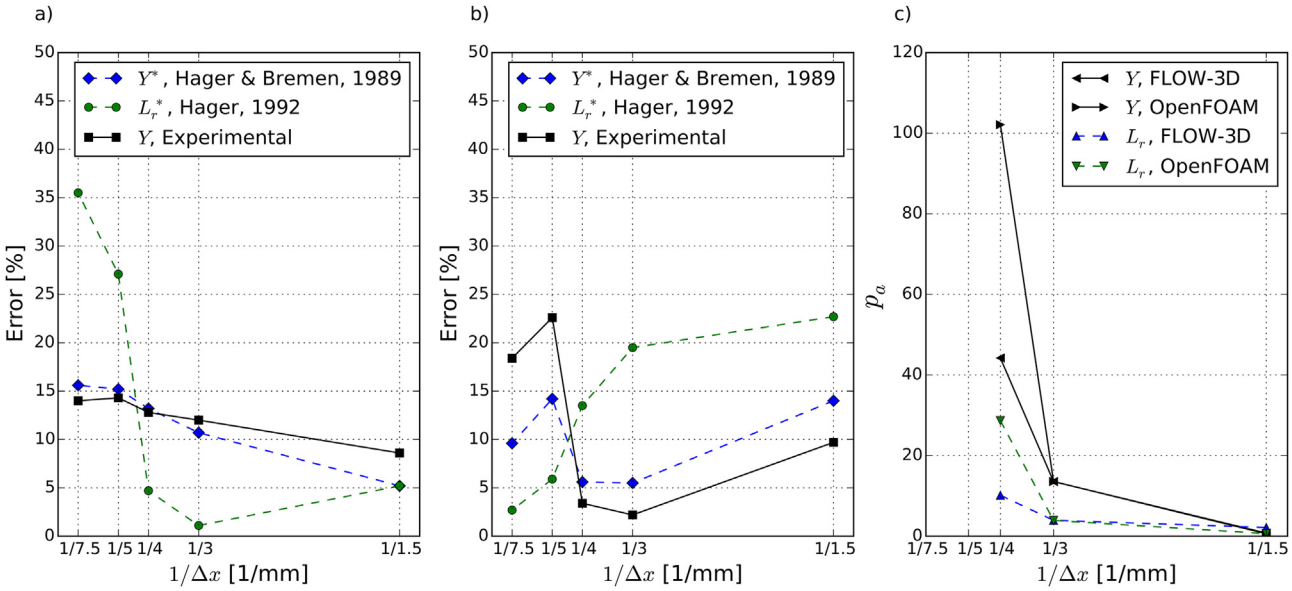

Fig. 3. Mesh sensitivity analysis. Model error in estimation of roller lengths (L_r^*) and sequent depths ratio, both according to experimental results (Y_e) and to Hager and Bremen (1989) (Y^*): a) OpenFOAM; b) FLOW-3D; c) Model apparent order (p_a), according to Celik et al. (2008).

model formal order in all cases. For this reason, all subsequent considerations regarding the quantitative analysis of results are exclusively referred to the 3mm mesh case. The numerical uncertainty of the model is assessed according to Celik et al. (2008) and spans from 6.0% to 6,7%. It is worth mentioning that, according to the results, FLOW-3D appears to be less dependent on mesh size variations than OpenFOAM.

4.2. Time-averaging window size sensitivity analysis

Most of the flows are essentially chaotic and so most of its characteristic variables show, in best case scenario, a statistically-stationary behavior. Hence, it is of paramount importance to extend the simulation time sufficiently and then average the variables in order to avoid bias in the model outcome. The authors observe that stability of the solution can be assumed when the residuals of all the variables drop below the 10^{-3} threshold and the water content of the whole modeled channel stays stable during at least 10s.

However, this is a rather empirical criterion. In order to ensure that the time-averaging window size does not affect results significantly, a sensitivity analysis is also conducted. Some oscillating variables are carefully observed, namely: jump toe position (x_0), roller end position (x_r) and subcritical flow depth (y_2). As a conclusion, it can be stated that the sampling period chosen of 10s captures several characteristic oscillation periods of these variables, so avoiding bias in the averaging process.

During this analysis, certain quasi-periodicity in the variables is observed (i.e. patterns can eventually be detected, although their characteristic period seems not to be constant). The autocorrelation function is computed to investigate whether the monitored variables show periodic behavior or not, and if so, what is the characteristic time scale of their oscillations. Fig. 4 shows how all variables are quasi-periodic. Indeed, the autocorrelation function of all variables tested shows an attenuation trend comparable to that of a sine wave with a characteristic time scale way smaller than the averaging window size. Further discussion on the fluctuating behavior of hydraulic jumps is conducted during the analysis of results.

5. Results and discussion

5.1. Graphical analysis

Both models managed to produce physically-consistent hydraulic jumps. A close observation of the results shows that all features expectable in hydraulic jumps of these characteristics can be identified: stable and compact appearance, gradual air detrainment, low wave generation, high vorticity within the roller, no flow detachment around the hydraulic jump toe, etc (Hager, 1992). At the end of hydraulic jumps, hydrostatic flow profiles are restituted.

5.2. Average variable analysis

The quantitative analysis of the hydraulic jump variables is conducted using the results of the case study described in Table 2. The sequent depth values are compared to the expression proposed by Hager and Bremen (1989) and yield accuracies of 89.3% and 94.5% for OpenFOAM and FLOW-3D, respectively. These variables, when compared to experimental results, yield accuracies of 88.0% and 97.8%, respectively.

The hydraulic jump efficiency is also better predicted by FLOW-3D (97.1%) than by OpenFOAM (94.6%). The fact that the same model estimates better sequent depths and efficiencies is normal to a certain extent, as both variables are strongly correlated and their estimation depends on how models treat momentum transfer.

Another important variable in the analysis of hydraulic jumps is the roller length (L_r). This variable is easier to determine as a flow stagnation region, where streamwise velocity tends to zero, can always be identified. Murzyn and Chanson (2009b) define the roller as the stretch of hydraulic jumps where the flow depth increases monotonically. Nevertheless, the stagnation point is used as criterion in the present work for it is easier to identify in CFD modeling.

FLOW-3D appears to be less accurate when estimating the roller length: this model achieved an accuracy of 80.5%, whereas OpenFOAM reached 98.9%, both compared to Hager (1992). Compared to Wang and Chanson (2015a,b), the accuracy decreased to 77.4% and 91.5% respectively. This variable shows the largest sensitivity to model parameters, such as mesh element size, as Fig. 3 shows. This

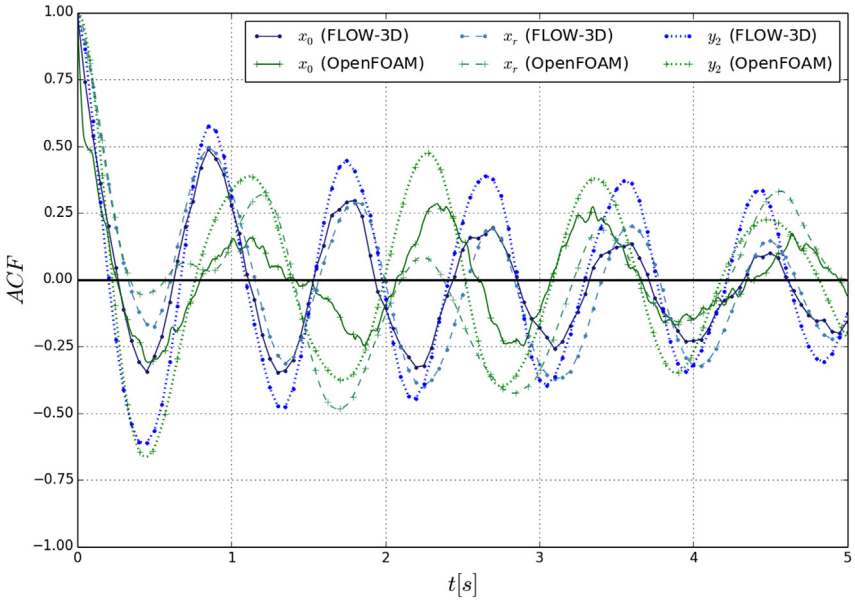

Fig. 4. Comparison of autocorrelation function (ACF) of hydraulic jump toe location (x_0), roller end position (x_r) and subcritical flow depth (y_2) in OpenFOAM and FLOW-3D.

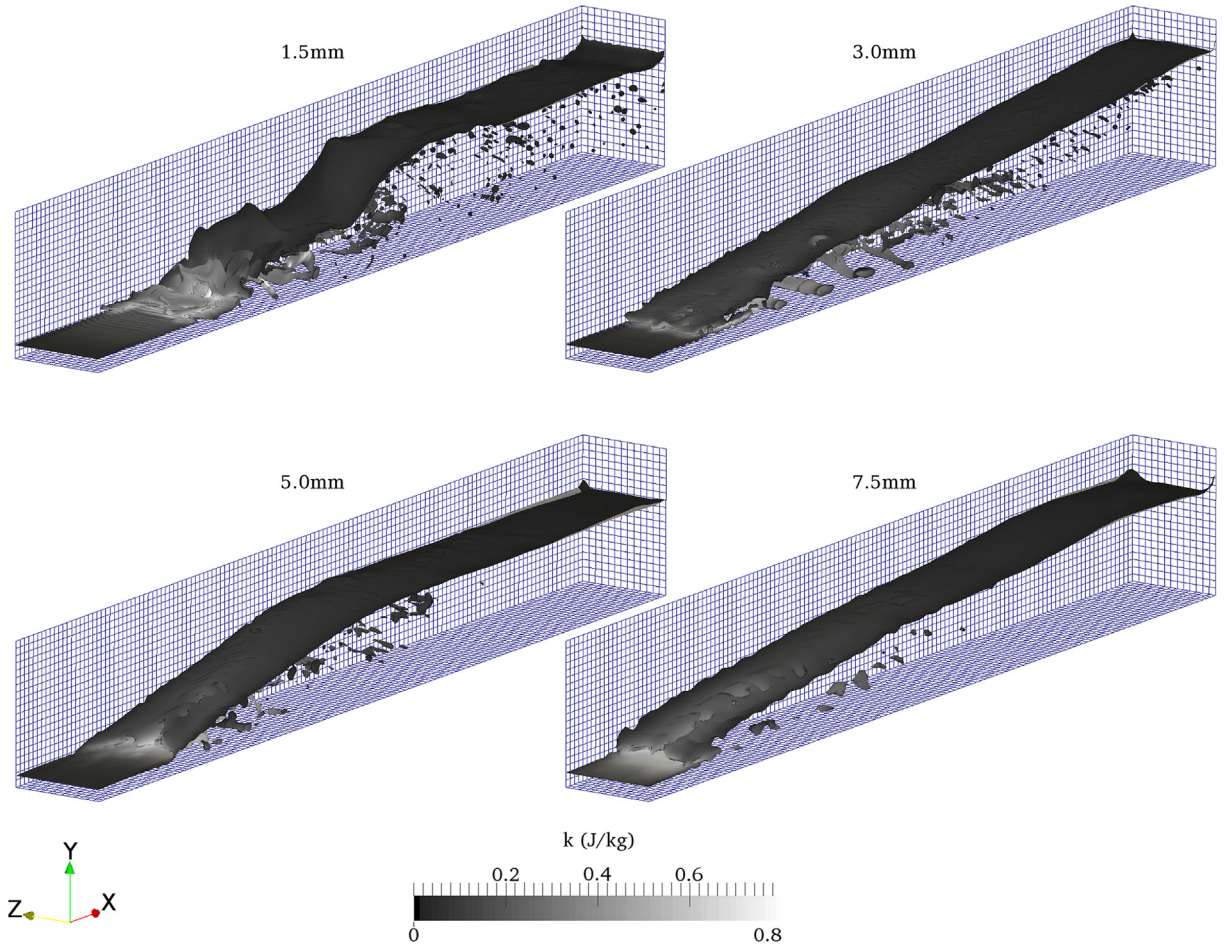

Fig. 5. Example of instant representation of numerically simulated hydraulic jumps, showing that different mesh sizes lead to different free surface profiles, TKE distributions and air entrapment patterns.

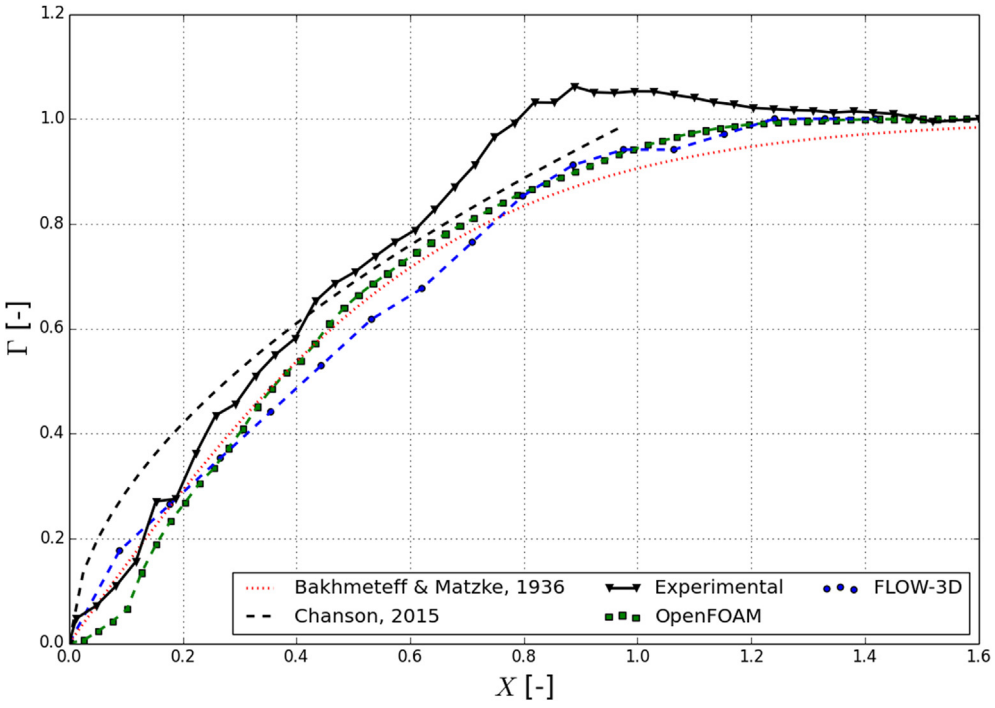

Fig. 6. Dimensionless free surface profile computed with OpenFOAM and FLOW-3D compared to Bakhmeteff and Matzke (1936), Chanson (2015) and experimental results.

makes model calibration and validation crucial as models must accurately predict where the roller is going to occur. It must be beared in mind that the largest energy release, shear stress and free surface fluctuation occur in this region, so its delimitation is of utmost importance in hydraulic engineering. Correct roller behavior estimations can avoid bank overflow issues and structure failure due to excessive dynamic loads.

As regards to the free surface profile throughout the hydraulic jump, it is also accurately defined by the models presented herein. Compared to the expression proposed by Bakhmeteff and Matzke (1936), OpenFOAM achieves a coefficient of determination of r^2=0.999 and FLOW-3D, r^2=0.988. Compared to more recent studies (Chanson, 2015), the coefficients of determination are r^2=0.962 and r^2=0.952, respectively. Compared to experimental results, the models yield accuracies of r^2=0.982 and r^2=0.966, respectively. The coefficient of determination (r^2) is commonly used to measure the efficiency of a model. This metric varies between 0 and 1.0, with perfect agreement for 1.0 (Bennett et al.,

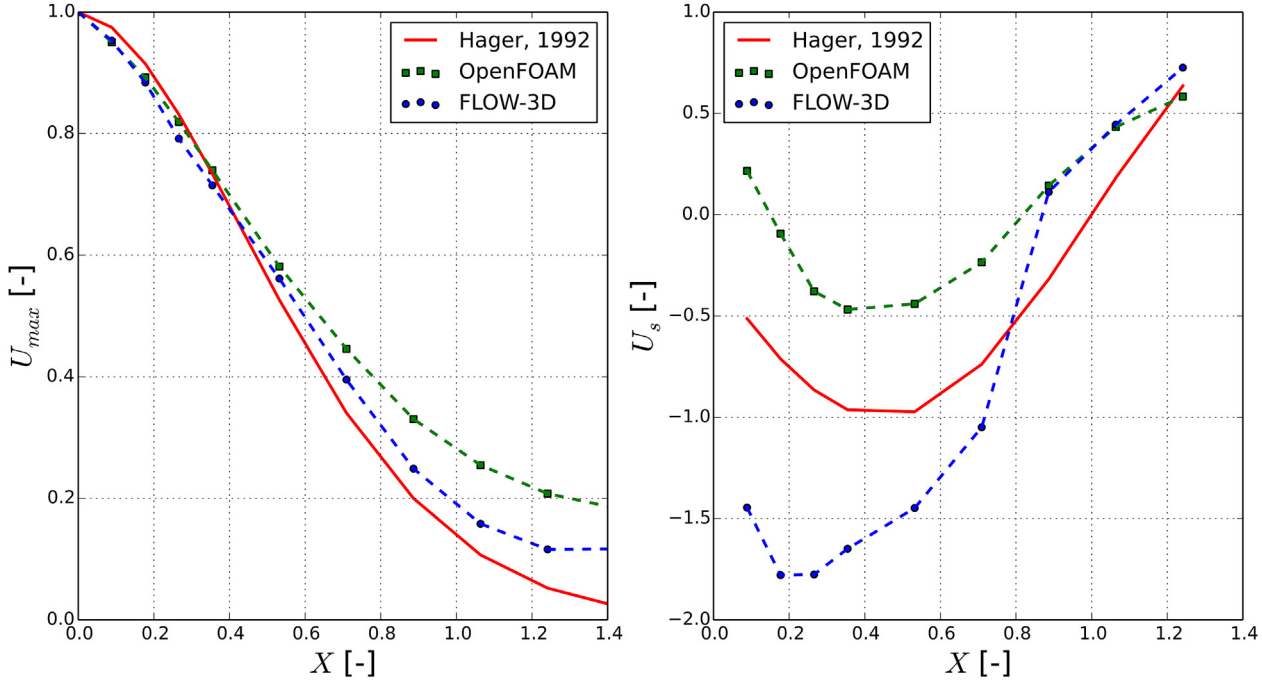

Fig. 7. Velocity analysis: a) Maximum velocity decay; b) Maximum backward velocity.

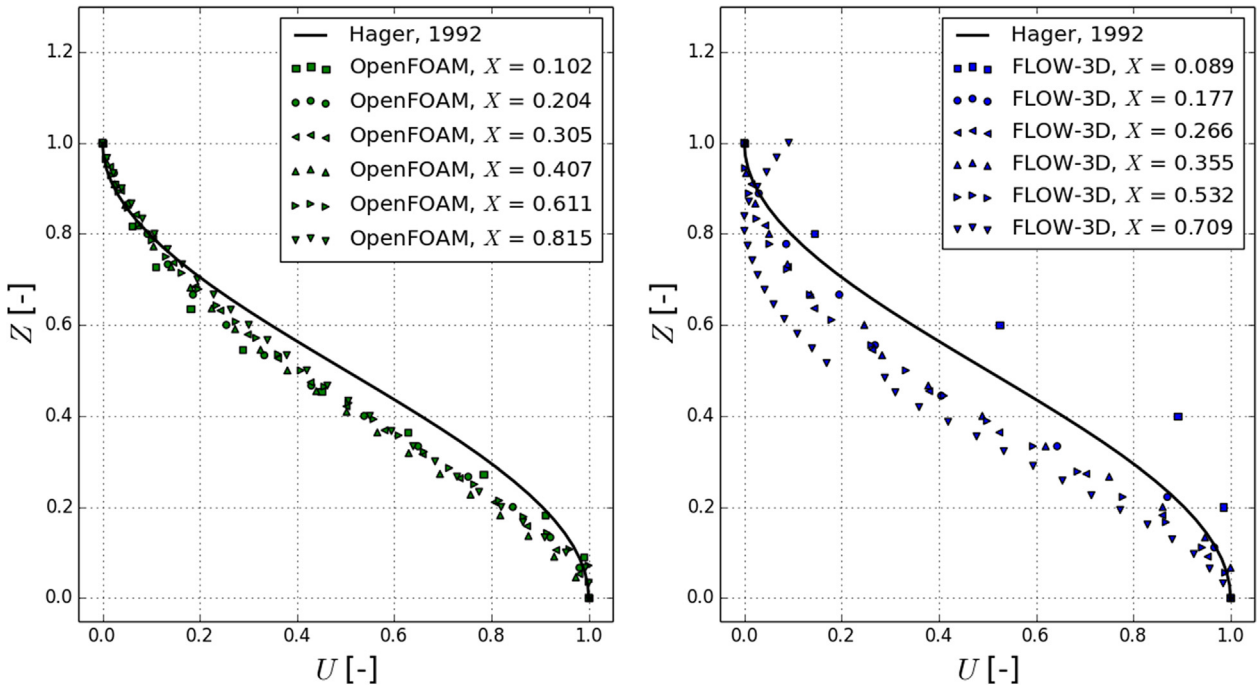

Fig. 8. Vertical velocity profiles along the longitudinal axis: a) OpenFOAM; b) FLOW-3D.

2013).

Fig. 6 shows the dimensionless free surface profile obtained by both codes compared to Bakhmeteff and Matzke (1936), Chanson (2015), and experimental results. It can be observed that numerically determined flow depths mostly fall between the profiles proposed by Bakhmeteff and Matzke (1936) and Chanson (2015). The slight overestimation of flow depths compared to Bakhmeteff and Matzke (1936), observable over X>1, is in agreement with experiments reported by Hager (1992). The experimental results follow the trend of all previously exposed free surface profiles. However, they show a sudden increase of flow depth around X~0.7, which is not observed in other profiles. A close observation of the images from which this profile is obtained points out that the most likely source of this mismatch is that large bubbles are expelled from the flow at this stretch, which cannot be filtered out by the surface detection algorithm. The bias caused by bubbles in the digital image treatment is currently being dealt with.

Concerning flow velocity distributions, Fig. 7 shows that the maximum differences with values reported by Hager (1992) occur for backward velocities (U_s). The flow processes in this region of hydraulic jumps are particularly complex. It is therefore expectable that the maximum errors take place in the swirling region, where turbulence models are most prone to fail in reproducing the flow behavior (Wilcox, 1998). Better accuracy can be expected for the rest of the analyzed flow variables. For the maximum velocity decay, FLOW-3D achieves higher degree of accuracy (99.7%) than OpenFOAM (99.5%) measured with the coefficient of determination (r^2). However, OpenFOAM yields better results than FLOW-3D in the estimation of backward velocities (88.2% and 83.7%) and vertical velocity profiles (97.6% and 90.3%), respectively. Anyway, these differences are rather small as both numerical codes reproduce the shape and main features fairly well as reported in the literature, as shown in Figs. 7 and 8. Table 3 summarizes the accuracy of all the results according to the variable analyzed and the model used. For this purpose, mean square relative error (MSRE) has been used where r^2 could not be applied (Bennett et al., 2013).

5.3. Time analysis

As mentioned above, the time domain analysis of certain hydraulic jump variables demonstrates that certain patterns tend to repeat in a periodic fashion, which is corroborated by the ACF

Table 3
Model accuracy summary. MSRE is mean square relative error and r^2 is coefficient of determination. Flow conditions are summarized in Table 2.

Variable	Referred to	Accuracy		Compared to
		OpenFOAM	FLOW-3D	
Y^*	1−MSRE	89.3%	94.5%	Hager and Bremen (1989)
Y_{Exp}		88.0%	97.8%	Experimental
L_r^*		98.9%	80.5%	Hager (1992)
L_r^*		91.5%	77.4%	Wang and Chanson (2015a,b)
η^*		94.6%	97.1%	Hager and Sinniger (1985)
Γ^*	r^2	0.999	0.988	Bakhmeteff and Matzke (1936)
Γ^*		0.962	0.952	Chanson (2015)
Γ_{Exp}		0.982	0.966	Experimental
U^*		0.976	0.903	Hager (1992)
U^*_{max}		0.995	0.997	Hager (1992)
U^*_s		0.882	0.837	Hager (1992)

analysis. In order to further infer this phenomenon, three variables are analyzed in the frequency domain using the Fast Fourier Transform (FFT), namely: jump toe position (x_0), roller end position (x_r), and subcritical flow depth (y_2). FFT converts data from temporal domain to frequency domain. This allows direct comparison of different temporal series in the frequency domain. This is of special interest in turbulence since repeating two temporal series representing the same phenomenon is impossible. Besides, transforming data can give insights into model performance that might not be obvious in untransformed data (Bennett et al., 2013). Fig. 9a, b, and 9c show the normalized power spectrum density (PSD) of these three variables according to the code used and the experimental data, respectively.

The analysis shows that the observed quasi-periodic oscillations have well defined periods. In fact, for the variables considered in the analysis of numerical results, a peak in each spectrum can be observed at a frequency around 1.0 Hz. The three variables analyzed oscillate at the same frequency according to the numerical code used. In the case of OpenFOAM, the dominant frequency is 0.90 Hz (period of 1.11s), whereas in FLOW-3D, the dominant frequency is 1.10 Hz (period of 0.91s), with an uncertainty of 0.1 Hz. The experimental data PSD (Fig. 9c) depicts slightly higher dominant frequencies for x_0 (1.6 Hz) and y_2 (2.9 Hz).

Despite of that, all these results compare well to previous works in terms of Strouhal number, showing certain correlation to Reynolds number (see Fig. 9d). It should be remarked that the similar dominant frequency found using both modeling approaches, not far from those experimentally determined, suggests that the regularity of the oscillating phenomena can be well described as a non-random and orderly process, which is superimposed on a background of turbulent random motion (Mossa, 1999). This fact obviously results from the complex relationship among vortex structures, internal features of the hydraulic jump and observable external variables.

5.4. Hydraulic jump length

In the present paper, a measureable variable is proposed to determine the hydraulic jump end position: the TKE decay. To obtain this variable, the values of TKE provided by the CFD models are estimated along the channel longitudinal axis, starting at the jump toe, where maximum values of TKE occur. An exponential decay for the TKE throughout the hydraulic jump is assumed:

$$k = k_{min} + (k_{max} - k_{min}) \cdot \exp(-\gamma [x - x_0]) \quad (10)$$

Where k_{min} is TKE asymptotic value that occurs downstream of the hydraulic jump, k_{max}, is TKE at the jump toe, γ quantifies the characteristic TKE decay along the hydraulic jump, and x_0 is the location of the jump toe. Using Eq. (10), the fraction of dissipated TKE throughout the hydraulic jump at a given x coordinate can be approximated as follows:

$$\sigma = 1 - \exp(-\gamma [x - x_0]) \quad (11)$$

For both model results; FLOW-3D and OpenFOAM, it is computed at which TKE decay value (σ) the hydraulic jump end must be placed to fulfill Bradley and Peterka (1957) hydraulic jump length criterion. Using least squares method, the characteristic decays obtained with OpenFOAM and FLOW-3D are γ_{OF}=6.293 J/(kg·m) and γ_{F3D}=4.915 J/(kg·m), respectively. It can be observed

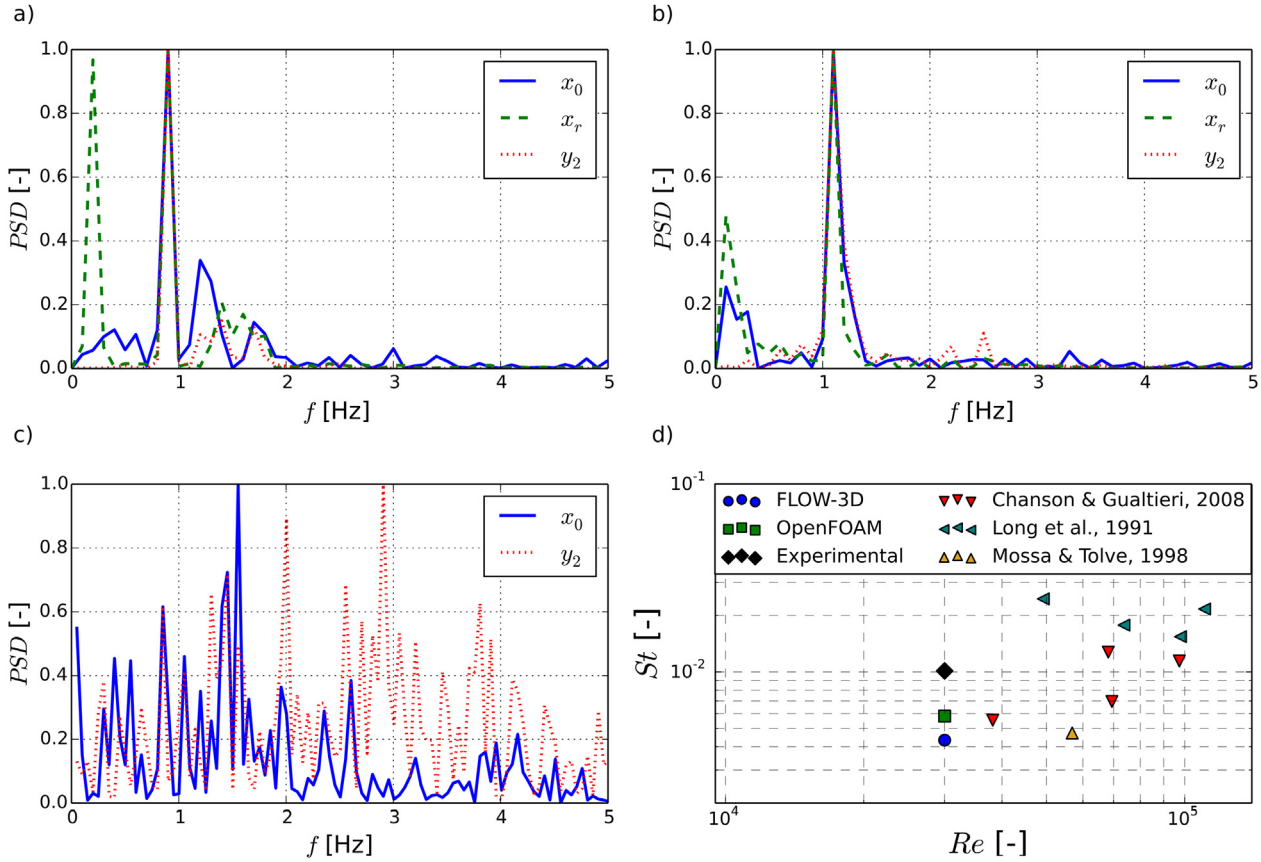

Fig. 9. Power spectrum density (PSD) of hydraulic jump toe location (x_0), roller end location (x_r) and subcritical depth (y_2): a) OpenFOAM; b) FLOW-3D; c) Experimental results; d) Comparison of resulting Strouhal numbers to previous studies.

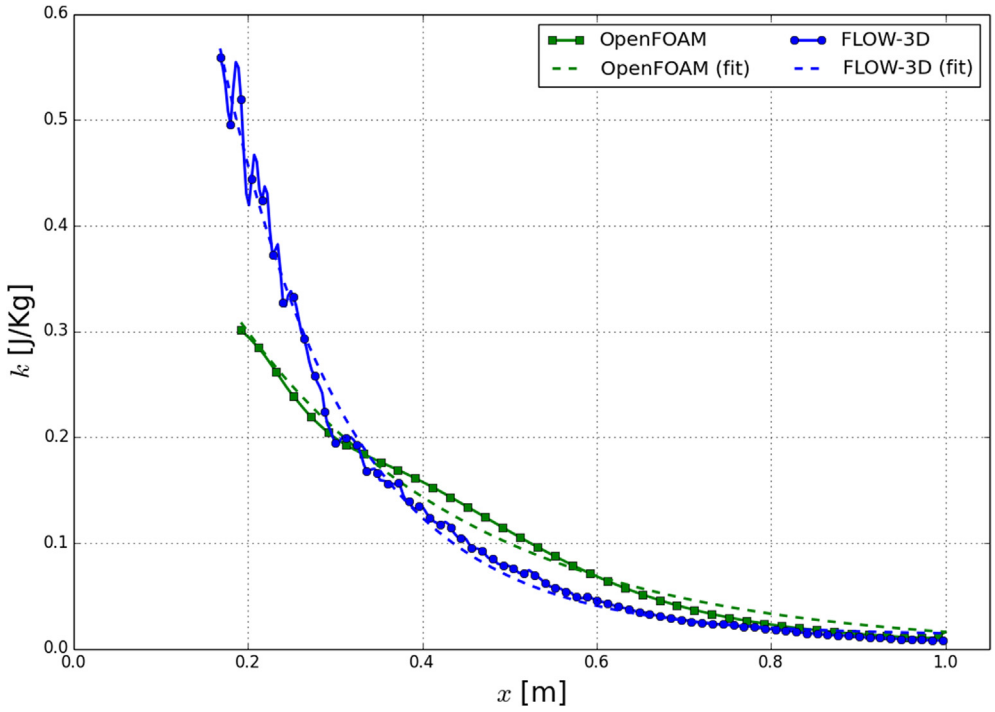

Fig. 10. TKE decay within the hydraulic jump along the longitudinal axis.

that the TKE minimum value (at the end of the hydraulic jump) is almost equal for both models (k_{min}=0.01 J/kg), although k_{max} differs significantly from one to another (Fig. 10). In particular, OpenFOAM yields $k_{max(OF)}$=0.302 J/kg, whereas FLOW-3D yields $k_{max(F3D)}$=0.559 J/kg.

The TKE decay threshold that makes hydraulic jump length (L_j) match with the expression by Bradley and Peterka (1957) is σ_{OF}=98.3% and σ_{F3D}=96.6% for OpenFOAM and FLOW-3D, respectively. Thus, a 95% decay of the maximum TKE could be established as an approximate threshold to define the jump end location in a numerical model.

Hydraulic jump length is a hard to determine variable and so involves a significant degree of uncertainty, no matter where the measurements are conducted: field, laboratory, or even numerical simulations, as it is the case analyzed herein (Chaudhry, 2007). This is basically due to the sudden changes in water surface level, linked to the formation of internal rollers and eddies. Several observable variables, such as velocity profile in the section or subcritical flow depths, can be used in practice to develop systematic criteria for determination of hydraulic jump end-section. Also, in the light of the results herein reported, TKE can also be used to this end.

6. Conclusions

Choosing the most suitable CFD code among the large amount of available options is crucial, but it can also be a tedious task as criteria are strongly case dependent. When modeling hydraulic structures, one of the most widely used codes has traditionally been FLOW-3D, although the open source platform OpenFOAM is also gaining use in this kind of applications. A similar CFD model is implemented using both codes and a classical hydraulic jump case at low Reynolds number is studied. In order to assess and compare both model accuracies, both experimental data and bibliography sources are used for validation purposes.

A mesh sensitivity analysis is conducted to determine the mesh cell size that provides a good compromise between accuracy and computational cost. Besides, as all the variables analyzed are highly variable in time, an analysis of the model sensitivity to the time-averaging window is conducted. Thus, results are not affected by the size of the averaging window. As a consequence of the latter analysis, certain quasi-periodic behavior is observed in some variables, such as the hydraulic jump toe location, the roller end location and the subcritical flow depth. Autocorrelation function has been employed to analyze the characteristic temporal length of the variable oscillation. Using FFT analysis, it is found that all these variables show similar dominant frequencies.

The comparison of the numerical model outcome to experimental and bibliography data shows that certain variables are best modeled by one code and others, by the other one. For instance, FLOW-3D appears to reproduce better the interaction between supercritical and subcritical flow and all derived variables, such as sequent depth ratio. However, OpenFOAM reproduces better the structure of the hydraulic jump. This can be observed in the more accurate estimation of the roller length. Regarding velocity fields, backward velocities and velocity profiles are slightly better reproduced by OpenFOAM, whereas the maximum velocity decay is better foreseen by FLOW-3D. However, major difficulties for both models arise in the roller region, where the swirling flow takes place. Fig. 11 summarizes clearly the accuracy of both codes according to the variable analyzed.

6.1. Future work

Major differences between the model estimates and previous works have been observed in the roller region, where strong recirculation takes place. The behavior of this region might be difficult to capture for the most commonly used turbulence models. However, this fact does not seem to exert a relevant effect on the overall description of the phenomenon (see Fig. 11 and Table 3). Anyway, modeling higher-Reynolds-number hydraulic jumps may improve current knowledge on turbulence model performance applied to the design of energy dissipation structures.

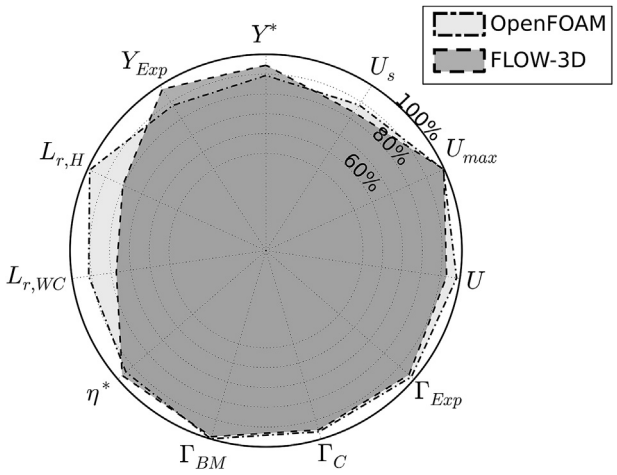

Fig. 11. Summary of code accuracies (%) of OpenFOAM and FLOW-3D.

As it can be observed in Fig. 5, CFD model parameters can exert significant effects on flow aeration. In this case, air entrapment and bubble size is obviously conditioned by mesh element size as noticed by other authors Witt et al. (2015). Other model parameters, such as turbulence model used, can also play an important role in flow aeration that so far, to the knowledge of the authors, has not been analyzed in depth and constitutes an interesting field of study. As mentioned above, the effects of flow aeration on hydraulic structure behavior are not negligible at all.

The fluctuation of certain hydraulic jump characteristic variables following visible patterns outlines possible further studies in this direction. CFD models can provide results at sufficient sampling rate to capture a wealth of phenomena related to the water surface turbulence and results can be compared to experimental data.

Acknowledgements

This research was supported by the VALi + D Scholarship Program (Generalitat Valenciana, Spain). We also greatly acknowledge financial support from the project BIA2011-28756-C03-01, "Natural and forced air entrainment in dam spillways and potential range of operation enlargement for hydraulic jump energy dissipators" (Spanish Ministry of Economy and Competitiveness) and from the ERDF European Union funding.

Nomenclature

Acronyms

CFD	Computational fluid dynamics
DNS	Direct numerical simulation
LES	Large eddy simulation
RANS	Reynolds averaged Navier–Stokes
RNG	Re-normalization group
VOF	Volume of fluid
FVM	Finite volume method
TKE	Turbulent kinetic energy
FFT	Fast Fourier transform
ACF	Auto correlation function
PSD	Power spectrum density

Sub- and super-indices

1	Relative to upstream of hydraulic jump
2	Relative to downstream of hydraulic jump
*	Relative to classic hydraulic jump
Exp	Relative to experimental results
t	Relative to turbulence
s	Relative to flow recirculation
min	Relative to minimum value
max	Relative to maximum value

Symbols

$x_i x_j x_k$	Cartesian coordinates
$u_i u_j u_k$	Velocity components
X	Dimensionless longitudinal coordinate
Z	Dimensionless vertical coordinate
U	Dimensionless velocity
t	Time
p	Pressure
ρ	Density
μ	Dynamic viscosity
υ	Kinematic viscosity
g	Acceleration of gravity
f	Frequency
f_b	Body forces
Q	q Water flow rate Specific flow rate
y	Flow depth
H	Hydraulic head
ΔH	Hydraulic head drop
Γ	Water free surface profile
b	Channel width
Y	Sequent depth
η	Hydraulic jump efficiency
x_0	Hydraulic jump toe position
x_r	Roller end position
x_j	Hydraulic jump end position
L_r	Roller length
L_j	Hydraulic jump length
α	Water fraction
k	Turbulent kinetic energy
ε	Turbulent kinetic energy dissipation rate
P_k	Production of TKE
$C_{1\varepsilon} C_{2\varepsilon} C_{3\varepsilon} \sigma_k \sigma_\varepsilon$	k-ε turbulence model parameters
d	Distance to wall
u_τ	Shear velocity
$x^+ y^+$	Dimensionless wall coordinates
ξ	Flow property
γ	TKE decay factor
σ	TKE threshold
r^2	Coefficient of determination
u_c	Compression velocity
Δx	Mesh element size
ω	Flow aspect ratio
δ_0	Distance from streambed to maximum velocity

Fluid mechanics numbers

Fr	Froude number
Re	Reynolds number
We	Weber number
Cr	Courant number

References

Ahmed, F., Rajaratnam, N., 1997. Three-dimensional turbulent boundary layers: a review. J. Hydraulic Res. 35 (1), 81–98.
Ashgriz, N., Poo, J., 1991. FLAIR: Flux line-segment model for advection and interface reconstruction. Elsevier J. Comput. Phys. 93 (2), 449–468.
Bakhmeteff, B.A., Matzke, A.E., 1936. .The hydraulic jump in terms dynamic similarity. ASCE Trans. Am. Soc. Civ. Eng. 101 (1), 630–647.
Balachandar, S., Eaton, J.K., 2010. Turbulent dispersed multiphase flow. Annu. Rev. Fluid Mech. 42 (2010), 111–133.
Bayon, A., Lopez-Jimenez, P.A., 2015. Numerical analysis of hydraulic jumps using

OpenFOAM. J. Hydroinformatics 17 (4), 662–678.
Belanger, J., 1841. Notes surl'Hydraulique, Ecole Royale des Ponts et Chaussees (Paris, France).
Bennett, N.D., Crok, B.F.W., Guariso, G., Guillaume, J.H.A., Hamilton, S.H., Jakeman, A.J., Marsili-Libelli, S., Newhama, L.T.H., Norton, J.P., Perrin, C., Pierce, S.A., Robson, B., Seppelt, R., Voinov, A.A., Fath, B.D., Andreassian, V., 2013. Characterising performance of environmental models. Environ. Model. Softw. 40, 1–20.
Berberovic, E., 2010. Investigation of Free-surface Flow Associated with Drop Impact: Numerical Simulations and Theoretical Modeling. Imperial College of Science, Technology and Medicine, UK.
Bidone, G., 1819. Report to Académie Royale des Sciences de Turin, séance. Le Remou et sur la Propagation des Ondes, 12, pp. 21–112.
Biswas, R., Strawn, R.C., 1998. Tetrahedral and hexahedral mesh adaptation for CFD problems. Elsevier Appl. Numer. Math. 26 (1), 135–151.
Blocken, B., Gualtieri, C., 2012. Ten iterative steps for model development and evaluation applied to computational fluid dynamics for environmental fluid mechanics. Environ. Model. Softw. 33, 1–22.
Bombardelli, F.A., Meireles, I., Matos, J., 2011. Laboratory measurements and multi-block numerical simulations of the mean flow and turbulence in the non-aerated skimming flow region of steep stepped spillways. Springer Environ. Fluid Mech. 11 (3), 263–288.
Bombardelli, F.A., 2012. Computational multi-phase fluid dynamics to address flows past hydraulic structures. In: 4th IAHR International Symposium on Hydraulic Structures, 9–11 February 2012, Porto, Portugal, 978-989-8509-01-7.
Borges, J.E., Pereira, N.H., Matos, J., Frizell, K.H., 2010. Performance of a combined three-hole conductivity probe for void fraction and velocity measurement in air–water flows. Exp. fluids 48 (1), 17–31.
Borue, V., Orszag, S., Staroslesky, I., 1995. Interaction of surface waves with turbulence: direct numerical simulations of turbulent open channel flow. J. Fluid Mech. 286, 1–23.
Boussinesq, J., 1871. Theorie de l'intumescence liquide, applelee onde solitaire ou de translation, se propageantdans un canal rectangulaire. Comptes Rendus l'Academie Sci. 72, 755–759.
Bradley, J.N., Peterka, A.J., 1957. The hydraulic design of stilling Basins : hydraulic jumps on a horizontal Apron (Basin I). In: Proceedings ASCE, J. Hydraulics Division.
Bradshaw, P., 1996. Understanding and prediction of turbulent flow. Elsevier Int. J. heat fluid flow 18 (1), 45–54.
Bung, D.B., 2013. Non-intrusive detection of air–water surface roughness in self-aerated chute flows. J. Hydraulic Res. 51 (3), 322–329.
Bung, D., Schlenkhoff, A., 2010. Self-aerated Skimming Flow on Embankment Stepped Spillways-the Effect of Additional Micro-roughness on Energy Dissipation and Oxygen Transfer. IAHR European Congress.
Caisley, M.E., Bombardelli, F.A., Garcia, M.H., 1999. Hydraulic Model Study of a Canoe Chute for Low-head Dams in Illinois. Civil Engineering Studies, Hydraulic Engineering Series No-63. University of Illinois at Urbana-Champaign.
Carvalho, R., Lemos, C., Ramos, C., 2008. Numerical computation of the flow in hydraulic jump stilling basins. J. Hydraulic Res. 46 (6), 739–752.
Celik, I.B., Ghia, U., Roache, P.J., 2008. Procedure for estimation and reporting of uncertainty due to discretization in CFD applications. ASME J. Fluids Eng. 130 (7), 1–4.
Chachereau, Y., Chanson, H., 2011. .Free-surface fluctuations and turbulence in hydraulic jumps. Exp. Therm. Fluid Sci. 35 (6), 896–909.
Chanson, H. (Ed.), 2015. Energy Dissipation in Hydraulic Structures. CRC Press.
Chanson, H., 2007. Bubbly flow structure in hydraulic jump. Eur. J. Mechanics-B/Fluids 26.3(2007) 367–384.
Chanson, H., Carvalho, R., 2015. Hydraulic jumps and stilling basins. Chapter 4. In: Chanson, H. (Ed.), Energy Dissipation in Hydraulic Structures. CRC Press, Taylor & Francis Group, ABalkema Book.
Chanson, H., Gualtieri, C., 2008. Similitude and scale effects of air entrainment in hydraulic jumps. J. Hydraulic Res. 46 (1), 35–44.
Chanson, H., Lubin, P., 2010. Discussion of "Verification and validation of a computational fluid dynamics (CFD) model for air entrainment at spillway aerators" Appears in the Canadian Journal of Civil Engineering 36(5): 826-838. Can. J. Civ. Eng. 37 (1), 135–138.
Chanson, H., 1994. Drag reduction in open channel flow by aeration and suspended load. Taylor & Francis J. Hydraulic Res. 32, 87–101.
Chanson, H., Montes, J.S., 1995. Characteristics of undular hydraulic jumps: experimental apparatus and flow patterns. J. hydraulic Eng. 121 (2), 129–144.
Chanson, H., Brattberg, T., 2000. Experimental study of the air–water shear flow in a hydraulic jump. Int. J. Multiph. Flow 26 (4), 583–607.
Chanson, H., 2013. Hydraulics of aerated flows: qui pro quo? Taylor & Francis J. Hydraulic Res. 51 (3), 223–243.
Chaudhry, M.H., 2007. Open-channel Flow, Springer Science & Business Media.
Chen, L., Li, Y., 1998. .A numerical method for two-phase flows with an interface. Environ. Model. Softw. 13 (3), 247–255.
Chow, V.T., 1959. Open Channel Hydraulics. McGraw-Hill Book Company, Inc, New York.
Daly, B.J., 1969. A technique for including surface tension effects in hydrodynamic calculations. Elsevier J. Comput. Phys. 4 (1), 97–117.
De Padova, D., Mossa, M., Sibilla, S., Torti, E., 2013. 3D SPH modeling of hydraulic jump in a very large channel. Taylor & Francis J. Hydraulic Res. 51 (2), 158–173.
Dewals, B., André, S., Schleiss, A., Pirotton, M., 2004. Validation of a quasi-2D model for aerated flows over stepped spillways for mild and steep slopes. Proc. 6th Int. Conf. Hydroinformatics 1, 63–70.
Falvey, H.T., 1980. Air-water flow in hydraulic structures. NASA STI Recon Tech. Rep. N. 81, 26429.
Fawer, C., 1937. Etude de quelquesécoulements permanents à filets courbes ('Study of some Steady Flows with Curved Streamlines'). Thesis. Imprimerie La Concorde, Lausanne, Switzerland, 127 pages (in French).
Gualtieri, C., Chanson, H., 2007. .Experimental analysis of Froude number effect on air entrainment in the hydraulic jump. Springer Environ. Fluid Mech. 7 (3), 217–238.
Gualtieri, C., Chanson, H., 2010. Effect of Froude number on bubble clustering in a hydraulic jump. J. Hydraulic Res. 48 (4), 504–508.
Hager, W., Sinniger, R., 1985. Flow characteristics of the hydraulic jump in a stilling basin with an abrupt bottom rise. Taylor & Francis J. Hydraulic Res. 23 (2), 101–113.
Hager, W.H., 1992. Energy Dissipators and Hydraulic Jump, Springer.
Hager, W.H., Bremen, R., 1989. Classical hydraulic jump: sequent depths. J. Hydraulic Res. 27 (5), 565–583.
Hartanto, I.M., Beevers, L., Popescu, I., Wright, N.G., 2011. Application of a coastal modelling code in fluvial environments. Environ. Model. Softw. 26 (12), 1685–1695.
Hirsch, C., 2007. Numerical Computation of Internal and External Flows: the Fundamentals of Computational Fluid Dynamics. Butterworth-Heinemann, 1.
Hirt, C., Nichols, B., 1981. .Volume of fluid (VOF) method for the dynamics of free boundaries. J. Comput. Phys. 39 (1), 201–225.
Hyman, J.M., 1984. Numerical methods for tracking interfaces. Elsevier Phys. D. Nonlinear Phenom. 12 (1), 396–407.
Juez, C., Murillo, J., Garcia-Navarro, P., 2013. Numerical assessment of bed-load discharge formulations for transient flow in 1D and 2D situations. J. Hydroinformatics 15 (4).
Keyes, D., Ecer, A., Satofuka, N., Fox, P., Periaux, J., 2000. Parallel Computational Fluid Dynamics' 99: towards Teraflops, Optimization and Novel Formulations. Elsevier.
Kim, J.J., Baik, J.J., 2004. A numerical study of the effects of ambient wind direction on flow and dispersion in urban street canyons using the RNG k–ε turbulence model. Atmos. Environ. 38 (19), 3039–3048.
Kim, S.-E., Boysan, F., 1999. Application of CFD to environmental flows. Elsevier J. Wind Eng. Industrial Aerodynamics 81 (1), 145–158.
Liu, M., Rajaratnam, N., Zhu, D.Z., 2004. Turbulence structure of hydraulic jumps of low Froude numbers. J. Hydraulic Eng. 130 (6), 511–520.
Lobosco, R., Schulz, H., Simoes, A., 2011. Analysis of Two Phase Flows on Stepped Spillways, Hydrodynamics - Optimizing Methods and Tools. Available from. : http://www.intechopen.com/books/hyd rodynamics-optimizing-methods-and-tools/analysis-of-two-phase-flows-on-stepped-spillways. Accessed February 27th 2014.
Long, D., Rajaratnam, N., Steffler, P.M., Smy, P.R., 1991. Structure of flow in hydraulic jumps. Taylor & Francis J. Hydraulic Res. 29 (2), 207–218.
Ma, J., Oberai, A.A., Lahey Jr., R.T., Drew, D.A., 2011. Modeling air entrainment and transport in a hydraulic jump using two-fluid RANS and DES turbulence models. Heat Mass Transf. 47 (8), 911–919.
Matos, J., Frizell, K., André, S., Frizell, K., 2002. On the performance of velocity measurement techniques in air-water flows. Hydraulic Meas. Exp. Methods 2002, 1–11. http://dx.doi.org/10.1061/40655(2002)58.
Meireles, I.C., Bombardelli, F.A., Matos, J., 2014. .Air entrainment onset in skimming flows on steep stepped spillways: an analysis. J. Hydraulic Res. 52 (3), 375–385.
McDonald, P., 1971. The Computation of Transonic Flow through Two-dimensional Gas Turbine Cascades.
Mossa, M., 1999. On the oscillating characteristics of hydraulic jumps, Journal of Hydraulic Research. Taylor &Francis 37 (4), 541–558.
Murzyn, F., Chanson, H., 2009a. Two-phase Gas-liquid Flow Properties in the Hydraulic Jump: Review and Perspectives. Nova Science Publishers.
Murzyn, F., Chanson, H., 2009b. Experimental investigation of bubbly flow and turbulence in hydraulic jumps. Environ. Fluid Mech. 2, 143–159.
Murzyn, F., Mouaze, D., Chaplin, J.R., 2007. Air–water interface dynamic and free surface features in hydraulic jumps. J. Hydraulic Res. 45 (5), 679–685.
Murzyn, F., Mouaze, D., Chaplin, J., 2005. Optical fiber probe measurements of bubbly flow in hydraulic jumps. Elsevier Int. J. Multiph. Flow 31 (1), 141–154.
Nagosa, R., 1999. Direct numerical simulation of vortex structures and turbulence scalar transfer across a free surface in a fully developed turbulence. Phys. Fluids 11, 1581–1595.
Noh, W.F., Woodward, P., 1976. SLIC (Simple Line Interface Calculation), Proceedings of the Fifth International Conference on Numerical Methods in Fluid Dynamics June 28-July 2. 1976 Twente University, Enschede, pp. 330–340.
Oertel, M., Bung, D.B., 2012. Initial stage of two-dimensional dam-break waves: laboratory versus VOF. J. Hydraulic Res. 50 (1), 89–97.
Olivari, D., Benocci, C., 2010. Introduction to Mechanics of Turbulence. Von Karman Institute for Fluid Dynamics.
Omid, M.H., Omid, M., Varaki, M.E., 2005. Modelling hydraulic jumps with artificial neural networks. Thomas Telford Proc. ICE-Water Manag. 158 (2), 65–70.
OpenFOAM, 2011. OpenFOAM: the Open Source CFD Toolbox User Guide. The Free Software Foundation Inc.
Peterka, A.J., 1984. Hydraulic design of spillways and energy dissipators. A water resources technical publication. Eng. Monogr. 25.
Pope, S.B., 2000. Turbulent Flows. Cambridge university press.
Pfister, M., 2011. Chute aerators: steep deflectors and cavity subpressure, Journal of hydraulic engineering. Am. Soc. Civ. Eng. 137 (10), 1208–1215.

Prosperetti, A., Tryggvason, G., 2007. Computational Methods for Multiphase Flow. Cambridge University Press.
Rajaratnam, N., 1965. The hydraulic jump as a Wall Jet. Proc. ASCE, J. Hydraul. Div. 91 (HY5), 107–132.
Resch, F., Leutheusser, H., 1972. Reynolds stress measurements in hydraulic jumps. Taylor & Francis J. Hydraulic Res. 10 (4), 409–430.
Romagnoli, M., Portapila, M., Morvan, H., 2009. Computational simulation of a hydraulic jump (original title, in Spanish: "Simulacioncomputacional del resaltohidraulico"), MecanicaComputacional, XXVIII, pp. 1661–1672.
Rouse, H., Siao, T.T., Nagaratnam, S., 1959. Turbulence characteristics of the hydraulic jump. Trans. ASCE 124, 926–966.
Rusche, H., 2002. Computational Fluid Dynamics of Dispersed Two-phase Flows at High Phase Fractions. Imperial College of Science, Technology and Medicine, UK.
Saint-Venant, A., 1871. Theorie du movement non permanent des eaux, avec application aux crues des rivieres et a l'introduction de mareesdansleurslits. Comptesrendus des seances de l'Academie des Sciences.
Schlichting, H., Gersten, K., 2000. Boundary-layer Theory. Springer.
Spalart, P.R., 2000. Strategies for turbulence modelling and simulations. Int. J. Heat Fluid Flow 21 (3), 252–263.
Speziale, C.G., Thangam, S., 1992. Analysis of an RNG based turbulence model for separated flows. Int. J. Eng. Sci. 30 (10), 1379–IN4.
Toge, G.E., 2012. The Significance of Froude Number in Vertical Pipes: a CFD Study. University of Stavanger, Norway.
Ubbink, O., 1997. Numerical Prediction of Two Fluid Systems with Sharp Interfaces. Imperial College of Science, Technology and Medicine, UK.
Valero, D., García-Bartual, R., 2016. Calibration of an air entrainment model for CFD spillway applications. Adv. Hydroinformatics 571–582. http://dx.doi.org/10.1007/978-981-287-615-7_38. P. Gourbesville et al. Springer Water.
Valero, D., Bung, D.B., 2015. Hybrid investigations of air transport processes in moderately sloped stepped spillway flows. In: E-Proceedings of the 36th IAHR World Congress, 28 June – 3 July, 2015 (The Hague, the Netherlands).
Van Leer, B., 1977. Towards the ultimate conservative difference scheme III. Upstream-centered finite-difference schemes for ideal compressible flow. J. Comput. Phys 23 (3), 263–275.
Von Karman, T., 1930. MechanischeAhnlichkeit und Turbulenz, Nachrichten von der Gesellschaft der WissenschaftenzuGöttingen. Fachgr. 1 Math. 5, 58–76.
Wang, H., Murzyn, F., Chanson, H., 2014a. Total pressure fluctuations and two-phase flow turbulence in hydraulic jumps. Exp. Fluids 55.11(2014) Pap. 1847, 1–16 (DOI: 10.1007/s00348-014-1847-9).
Wang, H., Felder, S., Chanson, H., 2014b. An experimental study of turbulent two-phase flow in hydraulic jumps and application of a triple decomposition technique. Exp. Fluids 55.7(2014) Pap. 1775, 1–18. http://dx.doi.org/10.1007/s00348-014-1775-8.
Wang, H., Chanson, H., 2015a. .Experimental study of turbulent fluctuations in hydraulic jumps. J. Hydraul. Eng. 141 (7) http://dx.doi.org/10.1061/(ASCE)HY.1943-7900.0001010. Paper 04015010, 10 pages.
Wang, H., Chanson, H., 2015b. Integral turbulent length and time scales in hydraulic jumps: an experimental investigation at large Reynolds numbers. In: E-Proceedings of the 36th IAHR World Congress 28 June – 3 July, 2015, The Netherlands.
Weller, H., Tabor, G., Jasak, H., Fureby, C., 1998. A tensorial approach to computational continuum mechanics using object-oriented techniques. Comput. Phys. 12, 620–631.
Wilcox, D., 1998. Turbulence Modeling for CFD, DCW Industries. La Canada, California (USA).
Witt, A., Gulliver, J., Shen, L., June 2015. Simulating air entrainment and vortex dynamics in a hydraulic jump. Int. J. Multiph. Flow 72, 165–180. ISSN 0301-9322. http://dx.doi.org/10.1016/j.ijmultiphaseflow.2015.02.012. http://www.sciencedirect.com/science/article/pii/S0301932215000336.
Wood, I.R., 1991. Air Entrainment in Free-surface Flows, IAHR Hydraulic Design Manual No.4, Hydraulic Design Considerations. Balkema Publications, Rotterdam, The Netherlands.
Yakhot, V., Orszag, S., Thangam, S., Gatski, T., Speziale, C., 1992. Development of turbulence models for shear flows by a double expansion technique, Physics of Fluids A: fluid Dynamics (1989-1993). AIP Publ. 4 (7), 1510–1520.
Youngs, D.L., 1984. An interface tracking method for a 3D Eulerian hydrodynamics code. Tech. Rep. 44 (92), 35–35.
Zhang, G., Wang, H., Chanson, H., 2013. Turbulence and aeration in hydraulic jumps: free-surface fluctuation and integral turbulent scale measurements. Environ. fluid Mech. 13 (2), 189–204.
Zhang, W., Liu, M., Zhu, D.Z., Rajaratnam, N., 2014. Mean and turbulent bubble velocities in free hydraulic jumps for small to intermediate froude numbers. J. Hydraulic Eng.